IOP Publishing Superconductor Science and Technology
Supercond. Sci. Technol. **26** (2013) 055008 (7pp) doi:10.1088/0953-2048/26/5/055008

Grain boundary segregation in a bronze-route Nb_3Sn superconducting wire studied by atom probe tomography

M J R Sandim[1], D Tytko[2], A Kostka[2], P Choi[2], S Awaji[3], K Watanabe[3] and D Raabe[2]

[1] Escola de Engenharia de Lorena—USP, 12602-810, Lorena, Brazil
[2] Max-Planck-Institut für Eisenforschung, D-40237, Düsseldorf, Germany
[3] Institute of Materials Research—Tohoku University, 980-8577, Sendai, Japan

E-mail: msandim@demar.eel.usp.br

Received 19 December 2012, in final form 19 February 2013
Published 26 March 2013
Online at stacks.iop.org/SUST/26/055008

Abstract

Atom probe tomography was used to characterize the A15 phase in a bronze-route Nb_3Sn superconducting wire with a bronze matrix composition of Cu–8Sn–0.3Ti (in at.%). We observed depletion of niobium and segregation of Cu and Ti atoms at Nb_3Sn grain boundaries. While the Nb depletion is about 15% relative to the grain interior, the average ratio between Cu and Ti excess values is 9 to 2. Segregation extends to a distance $d \sim 9$ Å from the point of maximum Cu and Ti concentrations. Such local variation in the stoichiometry at the grain boundary region can be an additional source of flux-pinning in the Nb_3Sn phase. Other microstructural parameters, such as the grain size and chemical composition of the Nb_3Sn layer, were investigated by electron backscatter diffraction and transmission electron microscopy.

(Some figures may appear in colour only in the online journal)

1. Introduction

Nb_3Sn, an intermetallic compound with A15-type crystal structure, is one of the most important superconducting materials for designing high magnetic field devices [1–4]. The A15-type structure exists over a wide range of compositions in the system $Nb_{1-\beta}Sn_\beta$, extending from 18 to 25.5 at.% Sn (or $\beta = 0.18$–0.255) [2–5]. The current-carrying capability of a superconducting wire depends largely on the pinning of magnetic flux-lines (or vortices). For the Nb_3Sn phase, it is well known that grain boundaries play a fundamental role in flux-pinning [1]. In particular, the maximum pinning force is related to the reciprocal value of grain size [1]. Therefore, a detailed knowledge of the grain structure, including grain size distribution, morphology and chemical composition, is essential for understanding and optimizing the superconducting properties of the compound [1].

A widely used manufacturing technology to produce Nb_3Sn multifilamentary wires is the so-called bronze method [6, 7]. In this approach, a rod of niobium is inserted in a Cu–Sn alloy (bronze) matrix and this arrangement is drawn into a filament form to large strains. After multiple steps of bundling, drawing, and restacking sequences a multifilamentary wire is obtained. The compound Nb_3Sn is then reacted by annealing the resulting wire at a temperature between 650 and 700 °C, sometimes even higher [3]. The restacking and repeated wire drawing acts in three ways: first, it provides short diffusion paths for the subsequent heat treatment; second, it provides very high Hall–Petch strengthening [8, 9]; and third, it yields fine filaments to reduce the hysteresis losses [10]. The Nb_3Sn phase forms as a layer at the interface between Nb and the surrounding Sn-rich bronze matrix by solid state diffusion. As a consequence of this diffusion process there is an inherent Sn gradient in the A15 layer in bronze-route filaments. A portion of the inner core can prevail as pure Nb, surrounded by the A15 reaction phase [3, 6, 7].

Since the 1980s it has been verified that the critical current density (J_c) of Nb_3Sn wires exposed to high magnetic fields is substantially increased by alloying with small additions of Ta and Ti to the superconducting filaments [11, 12]. Ti doping accelerates Sn diffusion along grain boundaries

and, therefore, reduces the possible reaction treatment temperature [11, 13–15]. As a result, the grain size of the Nb_3Sn layer is considerably decreased by the addition of small amounts of Ti (~1 at.%) into the bronze alloy [11]. Such a reduction in grain size strengthens the flux-pinning performance and, consequently, enhances J_c [11, 12, 15]. Nowadays, almost all commercial Nb_3Sn wires are alloyed with either Ti or Ta [2]. Ti doping can be performed either by alloying appropriate amounts of Ti to the Cu–Sn bronze or, alternatively, to the Nb filaments [12, 16, 17]. These two different methods have been named external and internal Ti doping methods, respectively [12, 17]. According to Tachikawa *et al* [16], Ti is more readily incorporated into the Nb_3Sn layer from the matrix than from the core.

The grain morphology and composition profile of the A15 layer in bronze-route Nb_3Sn wires have been studied by several authors [2, 17–19]. Typically, the filament cross-section is almost equally divided into two areas with very different grain morphology, namely, equiaxed and columnar grains near the interface with the matrix and the Nb core, respectively [2, 19]. Suenaga *et al* [18] reported on the chemical composition at and near the grain boundaries in bronze-processed Ti-free Nb_3Sn specimens (both tape and wire-shaped composites), which were heat treated so that the reaction synthesis of the Nb_3Sn compound was associated with significant grain growth. By using Auger electron spectroscopy, they reported that Cu is only present at grain boundaries and that the amounts of Nb and Sn at the grain boundaries are significantly different from those in the interior of the grains. Depletion in Nb and an enrichment of Sn at grain boundaries of about ~40% and ~20%, respectively, was observed. Also, they found that the spatial extent of the disordered Nb_3Sn due to the presence of Cu extends to up ~20 Å from the grain boundary [18]. More recently, Cantoni *et al* [17] reported on the chemical composition of the Ti-doped A15 phase in bronze-processed Nb_3Sn superconducting wires. These authors investigated wires obtained from both external and internal Ti doping methods using scanning transmission electron microscopy (STEM) in combination with energy dispersive x-ray (EDX) microanalysis. While they detected Cu in almost all grain boundaries, Ti was only detected at grain boundaries in wires that had been obtained by the internal Ti doping method [17]. In recent years, although extensive studies reported Ta and Ti alloying [11, 13–16] in bronze-processed wires, only Cantoni *et al* [17], to the best of our knowledge, reported Ti segregation at grain boundaries in the A15 phase. Impurity segregation is a very important issue for two reasons. First, grain boundary characteristics have a strong effect on flux-pinning in Nb_3Sn [1]. In particular, the mechanism of the Ti addition effect on J_c from a phase microstructure perspective is not yet well understood [20]. Second, the effect of alloying on diffusion and growth of the Nb_3Sn compound is still an open question, since both lattice and grain boundary diffusion give a reasonable contribution to the growth mechanism of Nb_3Sn via the bronze method [21].

In this work, we use atom probe tomography (APT) to investigate impurity segregation at Nb_3Sn grain boundaries in a superconducting wire obtained by the bronze method. APT is a high-resolution characterization technique that enables three-dimensional elemental mapping with near-atomic resolution, suitable for studies involving segregation at internal interfaces [22]. Other microstructural parameters of the investigated material, such as the grain size and chemical composition of the Nb_3Sn layer, were characterized by using EBSD (electron backscatter diffraction) and STEM-EDX techniques, respectively. The chosen wire for this investigation is a commercial bronze-route Nb_3Sn multifilamentary wire, for which Ti doping was performed by alloying with the bronze matrix. Due to excellent superconducting properties, this wire was identified as a new and promising candidate for fabrication of react-and-wind coils [3]. A detailed EBSD study for texture evaluation of the Nb_3Sn phase was conducted on a similar wire (same technical specification but from a different production batch) and was reported in a previous work [23].

2. Experimental details

The investigated wire was produced by Furukawa Electric Co. Ltd. It was 1 mm in diameter and contained 11 457 Nb_3Sn individual filaments embedded in a bronze matrix with a composition of Cu–8Sn–0.3Ti (in at.%). This wire was heat treated at 670 °C for 96 h, resulting in excellent superconducting properties with $J_c \sim 300$ A mm^{-2} at 16 T and $B_{c2} \sim 23.9$ T, at 4.2 K, where J_c is the critical current density and B_{c2} is the upper critical field [3]. More details about the design and superconducting properties of this wire can be found elsewhere [3, 24].

For EBSD mapping, both transversal and longitudinal cross-sections of the investigated wire were Ar-ion polished using the precision etching coating system GATAN—Model 682. EBSD data from Nb_3Sn filaments was determined by means of automated acquisition and further indexing of Kikuchi patterns after image processing with a TSL EBSD system interfaced to a JEOL JSM-6500F FEG-SEM.

Specimens for TEM analyses were prepared by using a JEOL JEM-9320 focused Ga^+ ion beam (FIB) system operated at 30 kV. TEM on the transversal cross-section of the wire was performed using a JEOL JEM-2200 FS operated at 200 kV for bright-field (BF) scanning TEM (STEM) imaging and EDX chemical analysis.

APT samples were prepared using a dual-beam focused ion beam (FEI Helios Nanolab 600). All samples were cut out from the central part of the A15 layer, with the axis of the APT sample parallel to the wire axis. Pulsed-laser APT was performed using a local electrode atom probe (LEAP™ 3000X HR, Cameca Instruments) at a specimen temperature of about 60 K. An ultrafast pulsed laser of ~10 ps pulse width and 532 nm wavelength was applied at a frequency of 250 kHz, where the laser pulse energy was set to 0.4 nJ and the target detection rate amounted to 1 atom per 1.25×10^5 pulses. Data analysis was performed using the IVAS software provided by Imago Scientific Instruments. The APT data sets analyzed in this work contained about 8 million ions. We used an evaporation field constant of 37 V nm^{-1} for the reconstruction of the APT data.

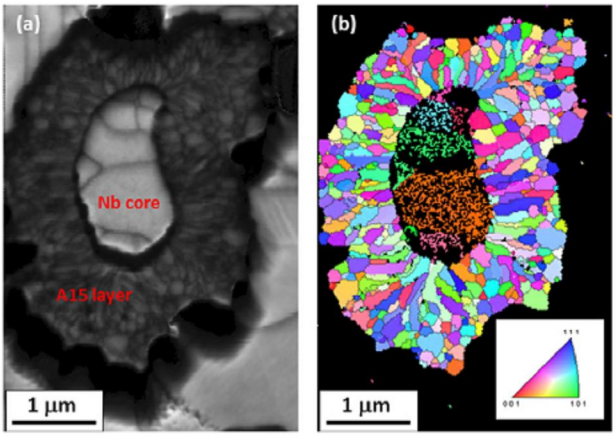

Figure 1. Microstructure of an individual Nb_3Sn filament in the cross-section of the investigated wire showing: (a) image quality map; and (b) corresponding inverse pole figure for A15 phase (EBSD).

3. Results and discussion

Figure 1 shows a typical Nb_3Sn filament in the transversal cross-section of the investigated wire. Figures 1(a) and (b) show the EBSD image quality and the corresponding grain boundary map of the A15 phase obtained by EBSD. From figure 1(a) the unreacted polycrystalline coarse grained Nb core is evident. The A15 layer exhibits a typical thickness of about 1.5 μm. Figure 1(b) shows elongated grains (near the Nb core) and equiaxed grains (near the matrix) in the microstructure of the Nb_3Sn phase that surrounds the coarse grained Nb core. EBSD maps of several Nb_3Sn filaments yield a mean grain size for the A15 phase of 99 ± 62 nm and 116 ± 56 nm for the transversal and longitudinal cross-section, respectively. Figure 1(b) also indicates that small areas of the Nb_3Sn phase are also found inside the Nb core. However, as discussed by Sandim *et al* [23], these areas are probably due to false indexing of low-quality diffraction patterns close to the Nb grain boundaries.

Figure 2 displays the chemical composition on a given Nb_3Sn filament obtained by EDX-TEM measurements. The EDX profile was taken over a line (see figure 2(a)) beginning inside the matrix and ending inside the Nb core. From figure 2(b) we see that the Sn content varies approximately from 15 to 23 at.% in the A15 layer and the detected Ti content is below 1.5 at.%.

In the following, we present APT results on samples cut out from positions inside the A15 layer of four different Nb_3Sn filaments, referred to as L1, L2, L3, and L4. Figure 3 shows the APT reconstruction of a representative sample, named L1. Figure 3(a) shows all elements mapped in the sample. We observe strong compositional changes at some of the grain boundaries, in particular fluctuations of the Ti and Cu concentration. Figures 3(b) and (c) show only the distribution of Cu and Ti atoms, respectively. Pronounced segregation of Cu and Ti to the grain boundaries is evident. In order to extract the grain boundary excess of Cu and Ti, we have analyzed the regions close to six grain boundaries, labeled GB1, GB2, GB3, GB4, GB5, and GB6 in figure 4(a).

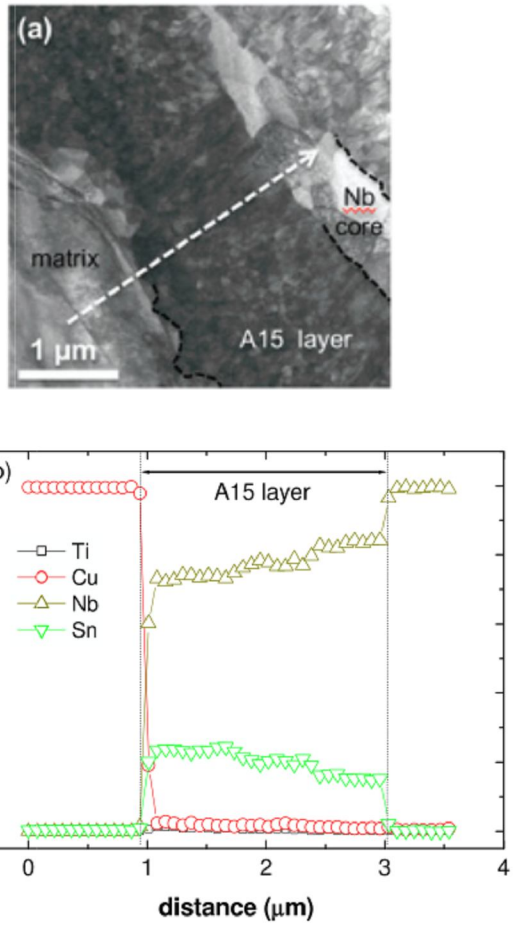

Figure 2. (a) Image of the cross-section of a given Nb_3Sn filament in the bronze matrix (TEM). The white line begins inside the matrix, crosses the A15 layer, and ends somewhere in the Nb core. The EDX profile taken over the white line is displayed in (b).

Figure 4(b) shows a clipped region containing GB1. In this figure, the brown iso-concentration surfaces close to interface indicate 1.5 at.% Cu. Such iso-concentration surfaces serve as a reference for constructing a proximity histogram or proxigram [25], displayed in figure 5 (the zero distance gives the position of the interface 1). From this proxigram an enrichment of Cu as well as a depletion of Nb at the grain boundary becomes evident. Considering the full-width at half-maximum of the Cu concentration, the width of such a GB segregation zone is ~1.8 nm, as defined in figure 5(b). We note that the width of the grain boundary segregation zone could be overestimated due to the local magnification effect [26] and the associated reconstruction artifact [27]. We can also calculate the mean grain boundary excess value (Γ) of Cu and Ti atoms using the following equation [28, 29]:

$$\Gamma_i = \frac{N_i}{e_{\mathrm{APT}} A_{\mathrm{GB}}}. \qquad (1)$$

where N_i is the excess number of element i segregated at the grain boundary, e_{APT} is the detector efficiency of the APT system (0.38) and A_{GB} is the grain boundary area. For the grain boundary displayed in figure 4(b), A_{GB} was taken as the average between the areas of iso-concentration

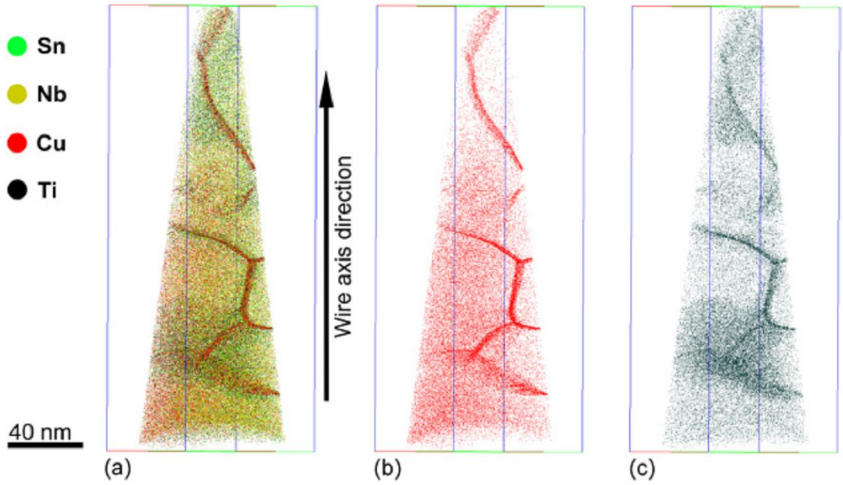

Figure 3. APT reconstruction of sample L1: (a) shows all chemical elements mapped in the sample and (b) and (c) show only Cu and Ti atoms, respectively.

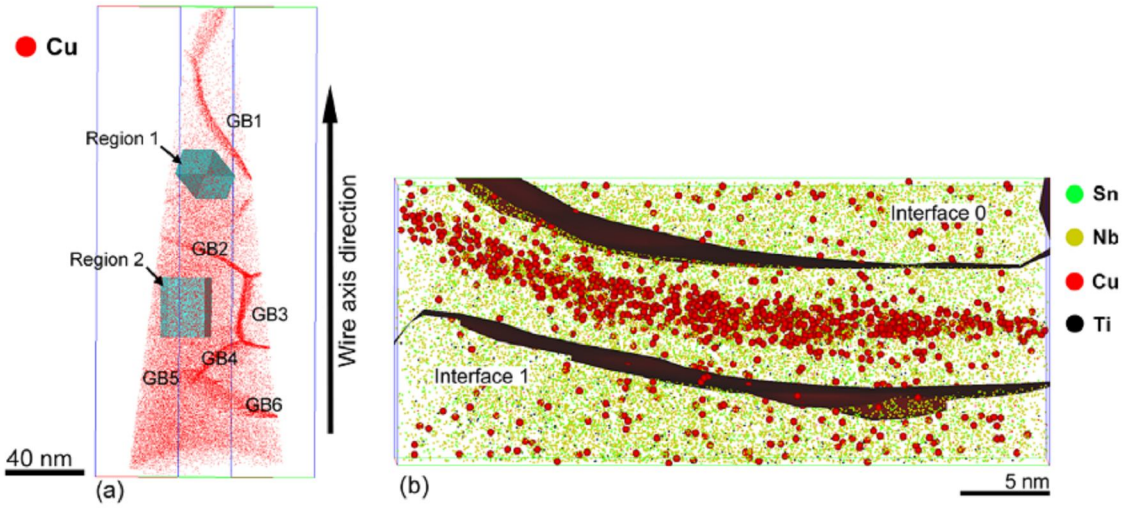

Figure 4. (a) APT reconstruction of sample L1 showing grain boundaries identified as GB1, GB2, GB3, GB4, GB5 and GB6 and two regions (labeled 1 and 2) far from the grain boundaries; (b) shows a clipped region containing GB1. The brown iso-concentration surfaces indicate 1.5 at.% Cu. The Cu atoms are enlarged for better visualization.

surfaces that delimitate the grain boundary, which gives an estimated value of 712 nm^2. The numbers of Cu and Ti atoms in the region delimited by the iso-concentration surfaces displayed in figure 4(b) are 2930 and 1026, respectively. Taking into account these values, from equation (1) we have calculated excess values of $\Gamma_{Cu} = 10$ atoms nm^{-2} and $\Gamma_{Ti} = 3$ atoms nm^{-2} at GB1. For GB2, GB3, and GB4 it was possible to get flat iso-concentration surfaces for >1.5 at.% Cu. Hence, we extracted the GB2, GB3, and GB4 region by choosing an iso-concentration value of 4.4 at.% Cu, 2.5 at.% Cu and 3.5 at.% Cu, respectively, and determined its excess values of Cu and Ti atoms. These results are in good agreement with those obtained for GB1 and will be shown later in this work. Also, their corresponding proxigrams (not shown) are similar to one obtained for GB1. For GB3 only we have detected some increase (~20%) in the Sn concentration across the grain boundary. The detected area of GB5 was too small to determine an accurate excess value and, therefore, is not given here. The proxigram across GB6, obtained with an 1.5 at.% Cu iso-concentration surface, is displayed in figure 6. From figure 6(a) we see that the Nb concentrations on both sides of GB6 differ from each other, where the Nb concentration is ~70 at.% to the left of GB6 and ~78 at.% in the opposite direction. Thus, the abutting grains have different compositions. The extent of the GB6 segregation zone, as determined from figure 6(b), is ~1.3 nm. From using equation (1) we have calculated an interface excess content of $\Gamma_{Cu} = 10$ atoms nm^{-2} and $\Gamma_{Ti} = 4$ atoms nm^{-2} for GB6, in good agreement with the corresponding results obtained for the other grain boundaries.

In order to check the amount of Cu far from the grain boundaries in sample L1 we clipped the regions (named 1 and 2) of interest corresponding to the grain interior, as indicated in figure 4(a). Table 1 shows the bulk composition of these clipped regions. From these data there is no trace of Cu far from the grain boundaries of the Nb_3Sn phase, in agreement

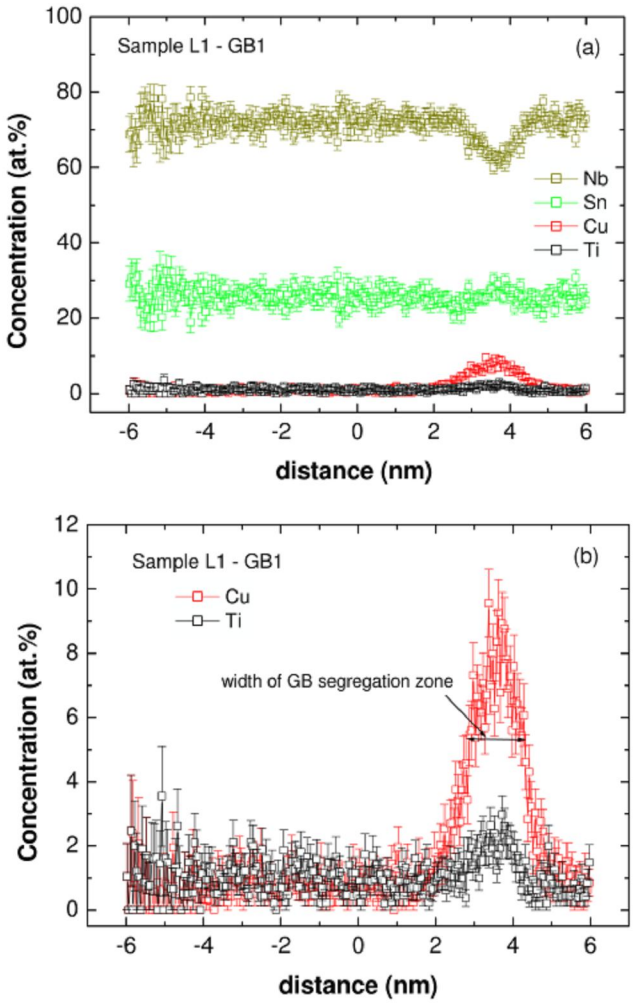

Figure 5. Proxigram related to GB1 in sample L1: (a) for all elements and (b) only for Cu and Ti. The width of GB segregation zone is defined as the full-width at half-maximum of the Cu concentration.

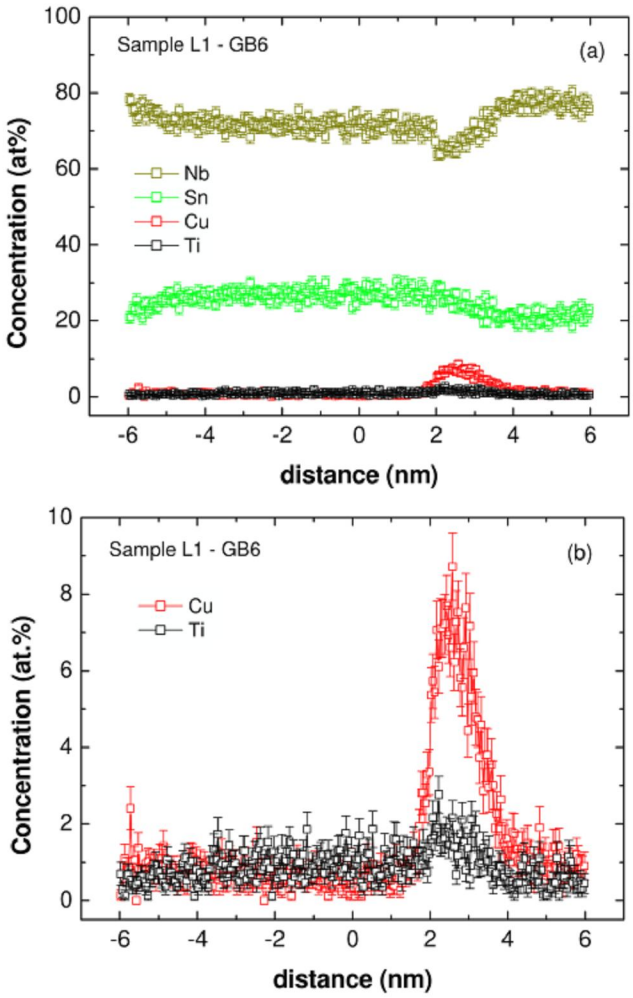

Figure 6. Proxigram related to GB6 in sample L1: (a) for all elements and (b) only for Cu and Ti.

Table 1. Sample L1: bulk composition of the regions 1 and 2 depicted in figure 4(a).

Ion type	Region 1 ranged (%)	Region 2 ranged (%)
Nb	81.5749	82.1794
Sn	18.2426	17.6402
Ti	0.1825	0.1805

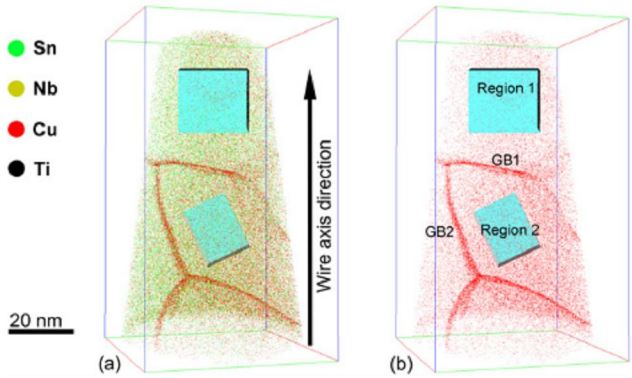

Figure 7. APT reconstruction of sample L2: (a) exhibits all elements mapped in the sample and (b) shows only Cu atoms. In (b) two grain boundaries are identified as GB1 and GB2 and regions 1 and 2 are clipped regions far from the grain boundaries.

with the observations reported by Suenaga *et al* [18] and Flükiger *et al* [2]. The appearance of a significant amount of Cu far from grain boundaries in the reconstructed map, as displayed in figure 3, is due to a background noise signal and peak overlap of Cu and Nb atoms in the APT mass-to-charge spectrum.

Figure 7 shows the APT reconstruction of a second analyzed sample, L2. We have obtained the bulk composition of the regions 1 and 2 indicated in figure 7(b) (not shown). Again, there is no trace of Cu far from the grain boundaries. As illustrated in figures 3 and 7, we find evidence of Cu and Ti segregation at grain boundaries in the Nb_3Sn phase in all samples. Following the same protocol as used for sample L1 we have determined the chemical composition across all the grain boundaries identified in the samples.

For samples L2, L3, and L4 we have analyzed two, one and two individual grain boundaries, respectively, using a 1.5 at.% Cu iso-concentration surface. For samples L2 and L3

Table 2. Measured width of GB segregation zone, Nb depletion and mean grain boundary excess value (Γ) of Cu and Ti atoms for grain boundaries investigated in samples L1, L2, L3 and L4. The symbols '*' and '**' mean Nb depletion when the grain boundary is reached, respectively, from left to right and in the opposite direction.

Sample	GB	Grain boundary extent (nm)	Nb depletion (%)	Γ_{Cu} (atoms nm ^{2})	Γ_{Ti} (atomsnm ^{2})
L1	GB1	1.7	13	10	3
	GB2	1.2	15	8	2
	GB3	2.2	16	13	4
	GB4	2.7	16	11	3
	GB6	1.3	8* or 15**	10	4
L2	GB1	2	11	9	1
	GB2	0.8	13	9	1
L3	GB1	1.9	11	10	3
L4	GB1	1.4	25* or 15**	8	1
	GB2	2.7	Not evident	11	3

the corresponding proxigrams (not shown) are similar to one displayed in figure 5. In sample L4, for one of the investigated grain boundaries, GB1, the proxigram (not shown) is similar to one displayed in figure 6. Also in this case we have found a slight change in Nb concentration on both sides of this particular grain boundary, where the Nb concentration is ~82 at.% to the left of GB1 (sample L4) and ~73 at.% on the opposite side. It is important to mention that the A15 phase is nanocrystalline, and compositional fluctuations can arise due to a non-equilibrium state. Despite the long annealing time, homogenization across some of the neighboring grains has not occurred yet. Another specific characteristic observed for GB1 in sample L4 is a relative change in the Sn concentration across the grain boundary, namely, of about 50%. For GB2 in L4 (not shown) no evidence of Nb depletion was found.

The main results of all samples are summarized in table 2. On average, we have found a Nb depletion of about 15% at grain boundaries of the A15 phase as well as segregation of Cu and Ti within a width of ~1.8 nm (18 Å). Such a distance means that, on average, the region of the non-stoichiometric Nb_3Sn extends to a length $d \sim 9$ Å from the point of maximum Cu and Ti concentrations (see figures 5 and 6). Except for two cases, no major changes were found for the Sn concentration across the Nb depleted A15 grain boundaries. These results are in partial agreement with those reported by Suenaga *et al* [18]. They detected substantial Nb depletion and Sn enrichment at grain boundaries of the A15 phase. Also, they found that the region of the disordered Nb_3Sn due to Cu segregation or a deficiency in Nb extends to ~20 Å from the grain boundary located at the point of maximum Cu concentration [18]. However, the specimen investigated by Suenaga *et al* [18] was heat treated under such conditions that Nb_3Sn formation was completed with significant grain growth, which is not the case for the Nb_3Sn wire investigated in this work.

In contrast to the bronze-route Nb_3Sn wires investigated by Cantoni *et al* [17], obtained using both internal and external Ti doping methods, the bronze matrix of the Nb_3Sn specimens investigated by Suenaga *et al* is a Cu–Sn alloy. There is no reference to alloying with Ti. In agreement with Suenaga *et al* [18] and Cantoni *et al* [17] we have also found Cu segregation at grain boundaries of the A15 phase in a bronze-route Nb_3Sn wire. In addition to Cu, we have systematically observed Ti segregation at the same grain boundaries, with a predominance of the former one. From table 2, the average ratio between the grain boundary excess values of Cu and Ti atoms in the A15 phase in the investigated bronze-route Nb_3Sn wire is 9 to 2. It is important to stress that the investigated wire in this work was obtained using external Ti doping, e.g., the Ti source is the bronze matrix. On the other hand, Cantoni *et al* [17] detected Ti only at the grain boundaries for wires obtained by the internal Ti doping method.

An exact knowledge of the chemical composition of the grain boundaries of the Nb_3Sn phase is very important for, at least, two reasons:

(a) The first one concerns the pinning force. It is well known that for the Nb_3Sn phase the maximum pinning force is inversely proportional to the grain size [1]. For the investigated Nb_3Sn multifilamentary wire the average grain size is about 100 nm, and agrees quite well with those reported by Godeke for commercial wires (100–200 nm) [1]. According to Suenaga *et al* [18], the variation in the concentration at the grain boundary region is an additional source of flux-pinning in the Nb_3Sn phase. Moreover, such a pinning contribution becomes stronger as the extent of the non-stoichiometric Nb_3Sn phase far from the grain boundary (located at the point of maximum Cu segregation) becomes closer to both electronic mean free path (l) and coherence length (ξ) of the A15 phase [18]. For pure Nb_3Sn it was found that l and ξ are ~50 and 30 Å, respectively [18]. In the present work, besides the Nb depletion, we have found both Cu and Ti segregation at grain boundaries with a segregation zone width of about $d \sim 9$ Å far from the point of maximum Cu and Ti concentrations. Since d. l, and ξ have a similar magnitude, the influence of the segregation on the flux-pinning strength of the investigated conductor should not be disregarded. It must be stressed that the exact influence of the segregation exerted by Ti and Cu on Nb_3Sn grain boundaries on the resulting flux-pinning force is not completely understood [1, 20].

(b) The latter, but no less important reason, concerns the diffusion mechanism for the growth of the Nb_3Sn compound. It is well known that Cu catalyzes the reaction to form the Nb_3Sn phase [30] and that the addition of Ti into the Cu–Sn alloy strongly affects the growth behavior of the Nb_3Sn layer [11, 14]. For the investigated bronze-route Nb_3Sn wire, in addition to Cu, we have found Ti segregation at the grain

boundaries of the Nb_3Sn phase. This experimental evidence shows that Ti also contributes to grain boundary disorder. According to Suenaga *et al*, disordered (lower symmetry) grain boundaries can enhance the diffusion of Sn along these interfaces [18]. As reported by Laurila *et al* [21], determining the diffusion mechanism in bronze-route Nb_3Sn is not a simple task. For the investigated wire, further experiments involving the APT characterization of specimens heat treated at lower annealing times should be conducted to clarify this issue.

Nevertheless, the results presented in this study contribute to visualizing three-dimensional segregation effects in Nb_3Sn with atomic resolution, being very important for the optimization of the superconducting properties of bronze-route Nb_3Sn multifilamentary wires.

4. Summary

We conducted APT analyses of a bronze-route Nb_3Sn superconducting wire (bronze matrix with composition Cu–8Sn–0.3Ti (in at.%)) that was heat treated at 670 °C for 96 h. APT provides atomic-scale information about Ti and Cu segregation at grain boundaries in the Nb_3Sn phase for bronze-route Nb_3Sn wires, which can be summarized as follows:

(1) At grain boundaries in the A15 phase, we find a Nb depletion of ~15% relative to the grain interior and pronounced segregation of Cu and Ti atoms to the Nb_3Sn grain boundaries. Far from the grain boundaries the Ti is incorporated into the Nb_3Sn phase and there is no trace of Cu inside the superconducting phase. These results are in reasonable agreement with those reported by other authors using locally resolving characterization techniques [2, 17, 18].

(2) In addition to Cu grain boundary segregation there is also Ti segregation, and the average ratio between the Cu and the Ti excess content at the grain boundaries is 9 to 2. Such segregation extends to a distance $d \sim 9$ Å from the point of maximum Cu or Ti concentration. Such a variation in the stoichiometry in the vicinity of grain boundaries can be an additional source of flux-pinning in the Nb_3Sn phase.

Acknowledgments

M J R Sandim is grateful to the Brazilian financial agency CNPq (Grant 201.112/2011-6) for supporting this research. The technical assistance of K Angenendt, M Nellessen, A Sturm and U Tezins (MPIE, Germany) is greatly appreciated. Thanks are also due to Furukawa Electric Co. Ltd (Japan) for supplying the superconducting Nb_3Sn-based wires for this investigation.

References

[1] Godeke A 2006 *Supercond. Sci. Technol.* **19** R68
[2] Flükiger R, Uglietti D, Senatore C and Buta F 2008 *Cryogenics* **48** 293
[3] Badica P, Awaji S, Nishijima G, Oguro H, Sandim M J R, Cangani M P, Ghivelder L, Katagiri K and Watanabe K 2007 *Supercond. Sci. Technol.* **20** 273
[4] Zhou J, Jo Y, Hawn Sung Z, Zhou H, Lee P J and Larbalestier D C 2011 *Appl. Phys. Lett.* **99** 122507
[5] Devantay H, Jorda J L, Decroux M, Muller J and Flükiger R 1981 *J. Mater. Sci.* **16** 2145
[6] Kaufman A R and Picket J J 1970 *Bull. Am. Phys. Soc.* **15** 833
[7] Tachikawa K, Itoh K, Kamata K, Moriai H and Tada N 1985 *J. Nucl. Mater.* **133/134** 830
[8] Hangen U and Raabe D 1995 *Acta Metall.* **43** 4075
[9] Heringhaus F, Raabe D and Gottstein G 1995 *Acta Metall.* **43** 1467
[10] Vostner A and Salpietro E 2006 *Supercond. Sci. Technol.* **19** S90
[11] Osamura K, Ochiai S, Kondo S, Namatame M and Nosaki M 1986 *J. Mater. Sci.* **21** 1509
[12] Senatore C, Abächerli V, Cantoni M and Flükiger R 2007 *Supercond. Sci. Technol.* **20** S217
[13] Mikami K and Kajihara M 2007 *J. Mater. Sci.* **42** 8178
[14] Hayase T and Kajihara M 2006 *Mater. Sci. Eng.* A **433** 83
[15] Abächerli V, Uglietti D, Seeber B and Flükiger R 2002 *Physica* C **372–376** 1325
[16] Tachikawa K, Sekine H and Iijima Y 1982 *J. Appl. Phys.* **53** 5354
[17] Cantoni M, Abächerli V, Uglietti D, Seeber B and Flükiger R 2008 *Microsc. Microanal.* **14** (Suppl 2) 1146
[18] Suenaga M and Jansen W 1983 *Appl. Phys. Lett.* **43** 791
[19] Wu I W, Dietderich D R, Holthuis J T, Hong M, Hassenzahl W V and Morris J W Jr 1983 *J. Appl. Phys.* **54** 7139
[20] Chaowu Z, Lian Z, Sulpice A, Soubeyroux J L, Xiande T, Verwaerde C and Hoang G K 2009 *Supercond. Sci. Technol.* **22** 065017
[21] Laurila T, Vuorinen V, Kumar A K and Paul A 2010 *Appl. Phys. Lett.* **96** 231910
[22] Miller M K and Forbes R G 2009 *Mater. Charact.* **60** 461
[23] Sandim M J R, Sandim H R Z, Zaefferer S, Raabe D, Awaji S and Watanabe K 2010 *Scr. Mater.* **62** 59
[24] Sandim M J R, Cangani M P, Sandim H R Z, Ghivelder L, Awaji S, Badica P and Watanabe K 2008 *IEEE Trans. Appl. Supercond.* **18** 1022
[25] Hellman O C, Vandenbroucke J A, Rusing J, Isheim D and Seidman D N 2000 *Microsc. Microanal.* **6** 437
[26] Miller M K and Hetherington M G 1991 *Surf. Sci.* **246** 442
[27] Vurpillot F, Bostel A and Blavette D 2000 *Appl. Phys. Lett.* **76** 3127
[28] Yoon K E, Noebe R D, Hellmam O C and Seidman D N 2004 *Surf. Interface Anal.* **36** 594
[29] Choi P, da Silva M, Klement U, Al-Kassab T and Kirchheim R 2005 *Acta Mater.* **53** 4473
[30] Godeke A 2005 *PhD Thesis* University of Twente, Enschede, The Netherlands